Available online at www.sciencedirect.com

ScienceDirect

journal homepage: www.elsevier.com/locate/he

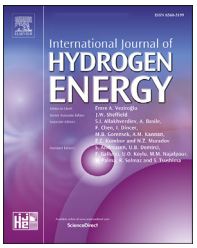

# Modeling hydrogen storage capacities, injection and withdrawal cycles in salt caverns: Introducing the GeoH$_2$ salt storage and cycling app

*Leopoldo M. Ruiz Maraggi*[*], *Lorena G. Moscardelli*

*Bureau of Economic Geology, The University of Texas at Austin*

## HIGHLIGHTS

- Open-source web application for modeling hydrogen storage and cycling processes in salt caverns.
- Hydrogen real gas thermodynamic simulator.
- Modeling capabilities include: physical properties, volumetric, withdrawal, injection, and cycling processes.

## ARTICLE INFO

*Article history:*
Received 21 October 2022
Received in revised form
17 March 2023
Accepted 19 March 2023
Available online xxx

*Keywords:*
Hydrogen geologic storage
Salt caverns
Web application
Thermodynamic simulator
Storage capacities
Cycling operations

## ABSTRACT

Salt caverns have been used as hydrogen ($H_2$) storage solutions in four locations worldwide with refineries and the petrochemical industry relying on these supplies as strategic back-up. The viability of storing $H_2$ within salt caverns is advantageous given their large volumetric capacities, their flexible operation with large injection and withdrawal rates, and for being a proven technology for the underground storage of a wide variety of gases and liquids. However, to our knowledge, there are no open-source web-based software tools to assess the technical potential of salt caverns for $H_2$ storage. This work aims to fill that gap by introducing the GeoH$_2$ Salt Storage and Cycling App, a computer program that models $H_2$ storage capacities, and injection/withdrawal cycles in salt caverns.

The GeoH$_2$ Salt Storage and Cycling App is a web-based thermodynamic simulator, which consists of the following modules: (a) $H_2$ physical properties, (b) volumetric, (c) production, (d) injection, and (e) cycling. The physical properties module provides the user with the main thermodynamic, transport, and thermal properties of $H_2$. The volumetric module allows the user to estimate $H_2$ storage capacities in salt caverns. The production and the injection modules simulate the withdrawal and the injection of $H_2$, respectively. Finally, the cycling module models sequential withdrawal and injection processes.

This study validates the results of the physical properties and the volumetric modules with real data. We validate the results of the production and the injection modules for synthetic cases using an open-source thermodynamic simulator.

This work presents a novel tool suitable to assess the technical potential of $H_2$ storage, injection, withdrawal, and cycling operations in salt caverns. This application can also be used, along with subsurface geological information, as a first order screening tool to assess $H_2$ storage capacity at a regional or hub scale.

© 2023 Hydrogen Energy Publications LLC. Published by Elsevier Ltd. All rights reserved.

* *Corresponding author.*
E-mail address: leo.ruiz@beg.utexas.edu (L.M. Ruiz Maraggi).

https://doi.org/10.1016/j.ijhydene.2023.03.293

0360-3199/© 2023 Hydrogen Energy Publications LLC. Published by Elsevier Ltd. All rights reserved.

Please cite this article as: Ruiz Maraggi LM, Moscardelli LG, Modeling hydrogen storage capacities, injection and withdrawal cycles in salt caverns: Introducing the GeoH$_2$ salt storage and cycling app, International Journal of Hydrogen Energy, https://doi.org/10.1016/j.ijhydene.2023.03.293

## Introduction

The shift in energy consumption from fossil-based fuels to renewable energy is reshaping the fabric of our energy systems. Hydrogen, a known energy carrier, can be used to help society bridge the gap between fossil fuels and renewable energies. However, a viable $H_2$ economy requires the development of several functional elements across the value chain including feedstock, production method, storage, transportation, and marketability (Fig. 1). Regarding storage, some estimates suggest that if $H_2$ gas were to replace 10% of U.S. natural gas, $H_2$ storage would need to be increased by a factor of 200 and these could be rather conservative numbers [1]. This emphasizes the need to increase $H_2$ storage capacity at a scale not seen before to fulfill the ambition to reach a net-zero economy in the next decade or two.

There are proven above and below ground $H_2$ storage options that include surface tanks, and subsurface lined rock and salt caverns. From these options, salt caverns provide the largest volumetric capacity for $H_2$ storage and therefore the best option to handle seasonal heat demand and to provide broader bulk power management solutions. Salt caverns can ensure both reliability and deliverability of high-power capacity during longer discharge times [2]. There are only four locations worldwide where $H_2$ storage in salt caverns exists, bedded salt formations in Teeside in the United Kingdom and three salt domes along the Gulf Coast of the United States:

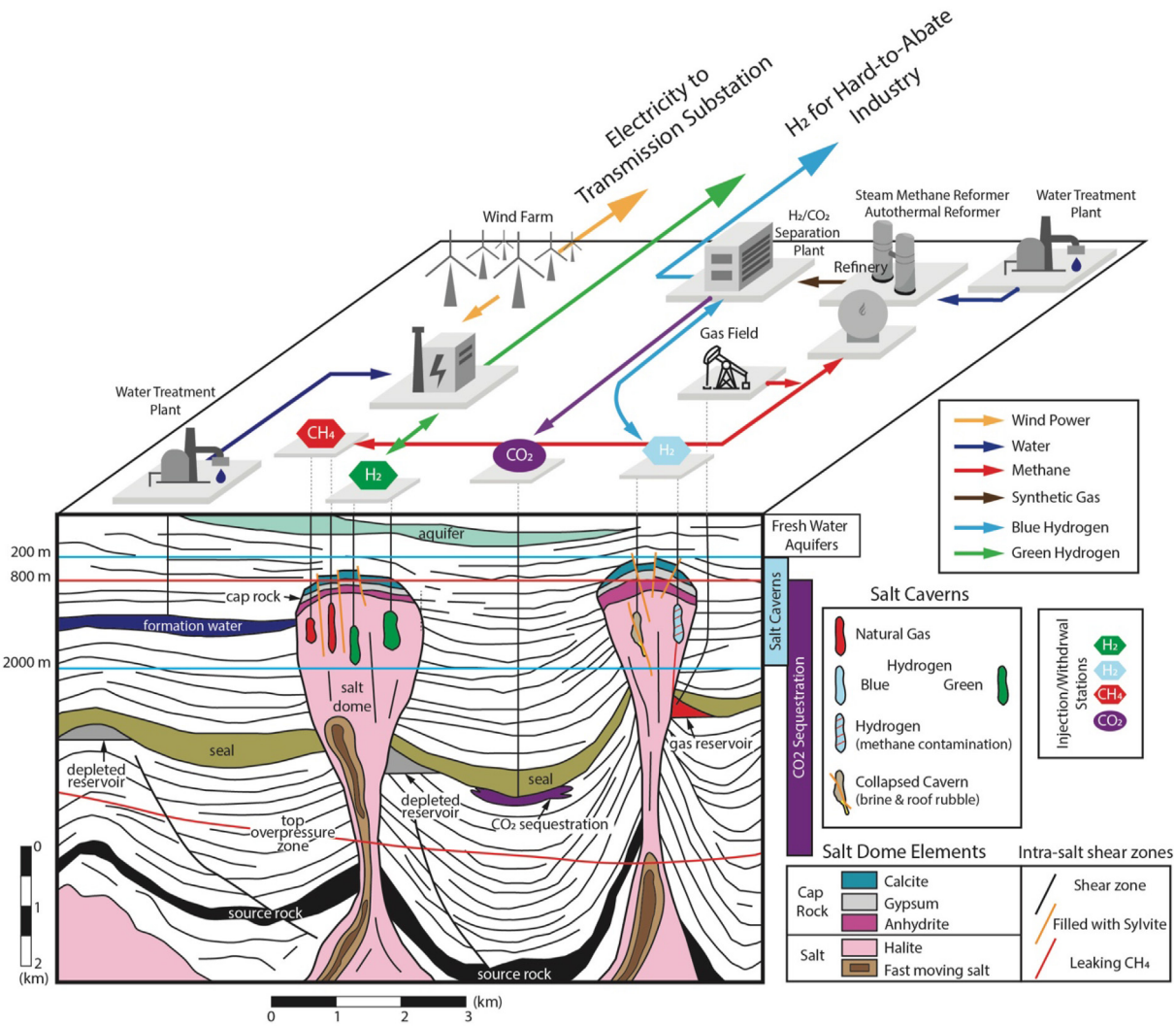


**Fig. 1 – Schematic rendition of above and below ground conditions and infrastructure necessary to facilitate the development of the $H_2$ economy. In addition to hydrogen storage in salt caverns, use of blue $H_2$ will require access to natural gas fields and proximity to steam methane reformers, as well as to subsurface conditions for carbon capture and sequestration. Likewise, use of green $H_2$ will require access to water resources, renewable energy and expensive electrolyzers. Key components will include the development of $H_2$ transportation networks, access to markets and implementation of safety standards. (For interpretation of the references to color in this figure legend, the reader is referred to the Web version of this article.)**

Please cite this article as: Ruiz Maraggi LM, Moscardelli LG, Modeling hydrogen storage capacities, injection and withdrawal cycles in salt caverns: Introducing the GeoH$_2$ salt storage and cycling app, International Journal of Hydrogen Energy, https://doi.org/10.1016/j.ijhydene.2023.03.293

Clemens Dome, Moss Bluff, and Spindletop [3]. These $H_2$ storage facilities are linked to oil refineries and fertilizer production but not to power generation.

The HyUnder project [4], funded by the European Union, evaluated the potential of different large-scale $H_2$ underground storage options such as salt caverns, depleted oil reservoirs, depleted gas reservoirs, aquifers, and lined rock caverns, among others. This research project [5] ranked salt caverns as the most feasible option for large-scale $H_2$ storage because of their relative integrity or tightness, their inertness to $H_2$ if the salt formation is predominantly halite, their high flexibility (large withdrawal and injection rates), and the relatively modest investment and operating costs. Currently, the European Union is funding the Hypster project [6] to demonstrate that the use of salt caverns for $H_2$ storage can be paired with renewable energy generation to help decarbonize industry and mobility. This project includes a pilot study in a repurposed cavern in France where high-frequency $H_2$ cycling is to take place in 2023. Hypster seeks to demonstrate the safety and low environmental impact associated with the use of salt caverns for $H_2$ storage and power generation. Results of this study will provide with a better understanding of desirable subsurface conditions to preserve the quality of the stored $H_2$, as well as to improve estimates associated with the cost of storing $H_2$ within salt caverns.

It is important to highlight that current $H_2$ storage sites experience infrequent hydrogen injection/withdrawal cycling. The stored $H_2$ in these facilities is meant to act as backup to avoid expensive refinery shutdowns due to $H_2$ supply disruptions. In contrast, in a scenario where $H_2$ storage is intended to mitigate renewable energy curtailment and intermittency, the frequency of injection/withdrawal cycles will increase to several cycles per year or month. Hydrogen storage in salt caverns for the purposes of power generation can be seen as the utilization of a large subsurface battery, but this comes with many challenges. Upscaling of the technology will require estimations of $H_2$ storage capacity for new sites based on subsurface conditions, as well as a better understanding of cavern's $H_2$ cycling limitations.

The development of the $H_2$ economy will require collocation of subsurface geological conditions and surface resources including proximity to infrastructure and markets (Fig. 1). Regions targeting green $H_2$ production will require high renewable power generation potential, and proximity to electrolyzers. On the other hand, regions interested in blue $H_2$ will require a steady supply of natural gas and proximity to refineries with steam methane reformers and separation plants to both produce $H_2$ and capture carbon dioxide respectively. In addition, blue $H_2$ production facilities need to be in close proximity to geological storage sites for permanent carbon dioxide sequestration. Blue and green $H_2$ production methods require large volumes of clean water, either as feedstock for green $H_2$, or as a source of steam for blue $H_2$ generation. The need to access clean sources of water for $H_2$ production can also pose a challenge depending on geographic location. All methods of $H_2$ production at scale will also require access to subsurface $H_2$ storage facilities, the presence of salt formations in the subsurface provide a solution to the $H_2$ storage problem by way of using salt caverns as a storage method. Unfortunately, salt formations are not ubiquitous and only certain geographic areas are suitable for the construction of salt caverns (Fig. 1). Finally, $H_2$ producing regions will require access to pipelines capable to transport $H_2$ to market; however, constructing new $H_2$pipelines and/or retrofitting existing natural gas pipelines is both challenging and costly.

Recent efforts regarding the development of simulators for modeling underground flow $H_2$ include [7–9]. However, these simulators are specifically designed for modeling flow of $H_2$ in porous media that assumes isothermal laminar flow (Darcy's law). However, flow modeling in salt caverns requires the incorporation of turbulent flow and the simulation of heat transfer effects between the cavern and the surrounding salt formation [10,11]. Current simulation challenges in salt caverns involve geomechanical modeling of creep transient closure, subsurface subsidence, and induced thermal tensile fractures during injection and withdrawal of $H_2$ [12,13].

The $GeoH_2$ Salt Storage and Cycling App is a modular web-based application that provides the user with a wide range of capabilities such as storage capacities and modeling of withdrawal, injection, and cycling operations in salt caverns. The modular nature of the $GeoH_2$ application allows the users to perform different calculations according to their interest. The web application consists of the following modules: (a) $H_2$ physical properties, (b) volumetric, (c) production, (d) injection, and (e) cycling. The physical properties module provides the user with the main thermodynamic, transport, and thermal properties of $H_2$. The volumetric module allows the user to estimate $H_2$ storage capacities in salt caverns. The production and the injection modules simulate the withdrawal and the injection of $H_2$, respectively. Finally, the cycling module models sequential withdrawal and injection operations.

## Introduction to the $GeoH_2$ salt storage and cycling web application

The $GeoH_2$ Salt Storage and Cycling App is a web-based thermodynamic simulator. It consists of five modules: (a) $H_2$ fluid properties, (b) volumetric, (c) production, (d) injection, and (e) cycling. The physical properties module provides the user with the main thermodynamic, transport, and thermal properties of $H_2$. The volumetric module allows the user to estimate $H_2$ storage capacities in salt caverns. The production and the injection modules simulate the withdrawal and the injection of $H_2$, respectively. Finally, the cycling module models sequential withdrawal and injection processes.

Fig. 2 shows the homepage of the $GeoH_2$ Salt Storage and Cycling App. The menu on the upper left side of the web application displays the different modules of the web application: fluid properties, volumetric, production, injection, and cycling. The user can access the different modules by clicking on their respective icons. Web version 1.0 of the $GeoH_2$ Salt Storage and Cycling App will be released as a public domain during the second quarter of 2023. The aim of this paper is to describe the application and the engineering and geoscience methods behind its formulation.

Each of the modules of the web application consists of two main sections: (a) a section in which the user has to populate

Please cite this article as: Ruiz Maraggi LM, Moscardelli LG, Modeling hydrogen storage capacities, injection and withdrawal cycles in salt caverns: Introducing the $GeoH_2$ salt storage and cycling app, International Journal of Hydrogen Energy, https://doi.org/10.1016/j.ijhydene.2023.03.293

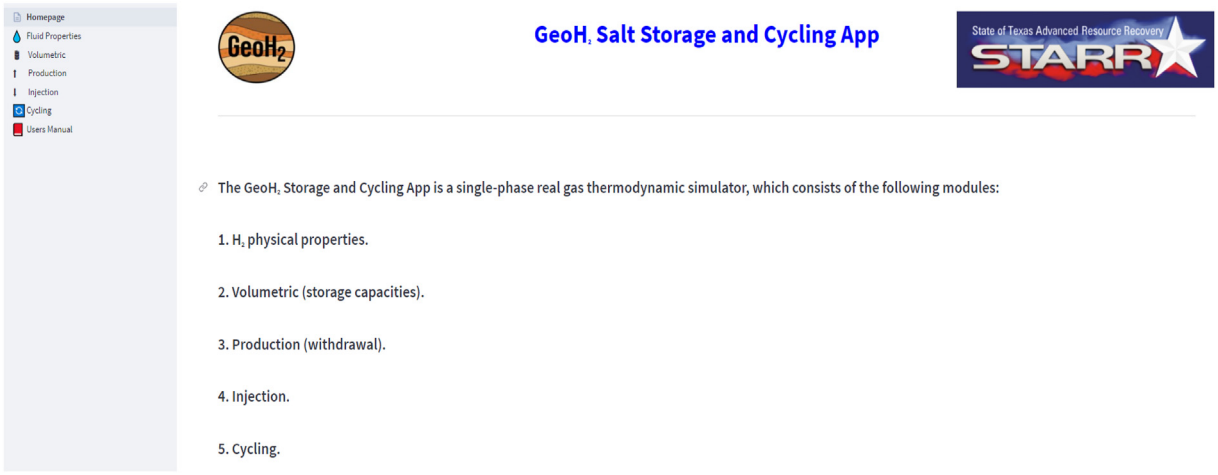


**Fig. 2 – Homepage of the $GeoH_2$ Salt Storage and Cycling App. The menu on the upper left side displays the different modules of the web application: fluid properties, volumetric, production, injection, and cycling. The user can access the different modules by clicking on their respective icons.**

the input variables, and (b) a section that presents the results of the performed calculations.

Fig. 3 illustrates the fluid properties module of the web application. Fig. 3a shows the input section of the module. The user needs to populate the input parameters, in this case: case name, temperature, and pressure, and then click on the RUN button to perform the calculations. Fig. 3b illustrates the output section of the fluid properties module presenting a table with the calculated properties. This table can be downloaded as a CSV file.

## Theory and calculations

This section provides a comprehensive description of the mathematical formulations used to perform the calculations for each of the following modules: (a) $H_2$ physical properties, (b) volumetric, (c) production, (d) injection, and (e) cycling. The $GeoH_2$ salt storage and cycling web application performs the calculations of the different modules using correlations to estimate thermodynamic, transport, and thermal properties of gaseous $H_2$ and macroscopic mass and energy balances [14].

Calculations for the different modules use the following assumptions: (a) single-phase single component gaseous $H_2$. We consider this assumption since $H_2$ is stored in current salt caverns with 95% purity [15], (b) perfect mixing: pressure and temperature are uniform within the cavern. The reasoning behind these assumptions are: the pressure gradient in the cavern can be neglected due to the low density of $H_2$ and the natural convection of $H_2$ leads to a constant temperature inside the cavern, (c) $H_2$ acts as cushion gas, (d) no presence of insolubles in the salt cavern. Insolubles might account up to 22% of the salt cavern volume [16], the user

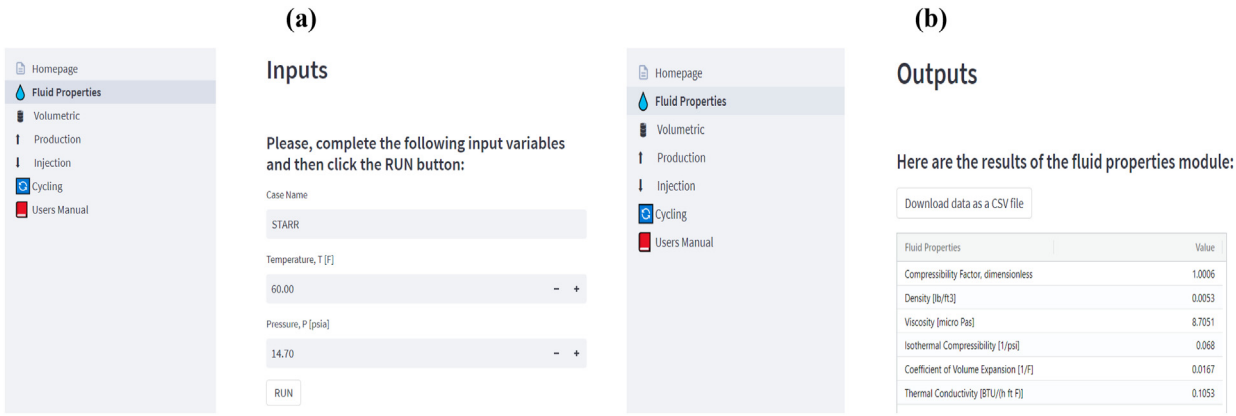


**Fig. 3 – Fluid properties module of the web application. Fig. 3a shows the input section of the module. The user needs to populate the input parameters, in this case: case name, temperature, and pressure, and then click on the RUN button to perform the calculations. Fig. 3b illustrates the output section of the fluid properties module presenting a table with the calculated properties. This table can be downloaded as a CSV file.**

Please cite this article as: Ruiz Maraggi LM, Moscardelli LG, Modeling hydrogen storage capacities, injection and withdrawal cycles in salt caverns: Introducing the $GeoH_2$ salt storage and cycling app, International Journal of Hydrogen Energy, https://doi.org/10.1016/j.ijhydene.2023.03.293

should consider this volume during the input of the height of the salt cavern, (d) all caverns have the same shape and volume, this assumption serves the purpose for screening storage capacity calculations, (e) the salt cavern volume remains constant throughout the entire withdrawal, injection, and cycling process, implying no volume changes with pressure and temperature. Future work plans to incorporate both elastic and viscoplastic behavior of salt, (f) salt rock has a constant thermal conductivity ($k_{salt}$) of 3.18 Btu/(h ft °F) [17], (g) for a given depth, the salt rock mass has a constant temperature 3.28 feet away from the cavern wall. This temperature along with the salt rock thermal conductivity are used to model the heat transfer between the cavern and the salt rock mass during injection, withdrawal, and cycling of $H_2$.

### Physical properties

This section describes the correlations used for calculating the thermodynamic, transport, and thermal properties of $H_2$.

#### Equation of state

The estimation of $H_2$ compressibility factor (Z), density ($\rho$), isothermal compressibility ($c_g$), and coefficient of volume expansion ($\beta$) are based on [18] equation of state (EOS).

$$Z(T,P) = 1 + \sum_{i=1}^{9} a_i \left(\frac{180R}{T(R)}\right)^{b_i} \left(6894.75\,\frac{P(psi)}{1\,psi}\right)^{c_i}, \tag{1}$$

where $a_i$, $b_i$, $c_i$ are the empirical coefficients of the correlation, see Ref. [18].

The real gas density uses Eq. (1) to estimate the $H_2$ compressibility factor Z.

$$\rho\,(T,P) = \frac{P\,Mr}{Z(T,P)\,RT}, \tag{2}$$

where $R$ is the ideal gas constant (1.985 Btu $R^{-1}$ $lbmol^{-1}$) and $Mr$ is the molecular weight of $H_2$ (2.016 lb/lbmol). The definition of the isothermal compressibility [19] is given by Eq. (3).

$$c_g = \frac{1}{\rho}\left(\frac{\partial \rho}{\partial P}\right)_T = \frac{1}{P} - \frac{1}{Z}\left(\frac{\partial Z}{\partial P}\right)_T. \tag{3}$$

Finally, the definition of the coefficient of volume expansion [19] is given by Eq. (4).

$$\beta = -\frac{1}{\rho}\left(\frac{\partial \rho}{\partial T}\right)_P = \frac{1}{T} + \frac{1}{Z}\left(\frac{\partial Z}{\partial T}\right). \tag{4}$$

Equations 3 and 4 are calculated using the $H_2$ compressibility factor Eq. (1).

#### Gas viscosity

The program estimates the $H_2$ gas viscosity using [20] correlation, Eq. (5).

$$\mu(T,\rho) = \mu_0(T) + \Delta\mu_{excess}(T,\rho) + \Delta\mu_{crit}(T,\rho). \tag{5}$$

Equation (5) includes a base estimation $k_0$ of the viscosity of $H_2$ at the limit of zero density, the term $\Delta\mu_{excess}$ accounts for the increase in viscosity at elevated density, and correction factor $\Delta\mu_{crit}$ represents the contribution of all other higher-order effects to the viscosity of the fluid at elevated densities including many body collisions and molecular-velocity correlations. For further details related to the coefficients of this correlation refer to Ref. [20].

#### Gas thermal conductivity

This work uses the [21] correlation for the thermal conductivity of $H_2$.

$$k = k_0(T) + \Delta k_{excess}(T,\rho) + \Delta k_{crit}(T,\rho). \tag{6}$$

The terms in Eq. (6) have the same physical meaning that in Eq. (5); they represent the contributions of thermal conductivity at the limit of zero density $k_0$, a correction for elevated density $\Delta k_{excess}$ , and the contributions of all other high-order effects $\Delta k_{crit}$.

### Volumetric calculations

The volumetric module estimates $H_2$ storage capacities in salt caverns. The module calculates storage capacities for a single cavern or multiple caverns given the salt dome geometry based on [22]. This method assumes that all caverns in a given dome have the same geometry. Given the geometry of the cavern and the salt dome, the module computes the following variables.

1. Number of salt caverns that can be built per salt dome using [22] method.
2. Geometric volume per cavern and for the total number of caverns.
3. Working gas volume per cavern and for the total number of caverns.
4. $H_2$ combustion energy (based on the $H_2$ lower heating value) per cavern and for the total number of caverns.
5. $H_2$ mass per cavern and for the total number of caverns.

The module can perform the calculations for cylindrical or spherical salt caverns. Cylindrical caverns model the shape of caverns in salt domes and spherical caverns represent caverns in bedded salt formations.

Fig. 4 illustrates the key parameters for modeling $H_2$ storage in salt caverns and the geometric parameters that are inputs for the volumetric calculations. These input parameters are: (a) salt dome diameter $D$, (b) cavern diameter $d$, (c) cavern height $h$, (d) edge length $L$ (distance between centers of adjacent caverns).

#### Total number of caverns

Equation (7) computes the total number of caverns $n$, given the salt dome diameter $D$ and the edge length $L$ (see Fig. 4).

$$n(D,L) = \frac{\pi\left(\frac{D}{2} - \sqrt{1/2}\,L\right)^2}{L^2}. \tag{7}$$

#### Effective number of caverns

Equation (8) calculates the effective number of caverns $n_{eff}$, given the total number of caverns $n$ and the fraction of caverns being built $f_{built}$. The effective number of caverns is a fraction of the total number of caverns.

$$n_{eff} = f_{built}\,n. \tag{8}$$

Please cite this article as: Ruiz Maraggi LM, Moscardelli LG, Modeling hydrogen storage capacities, injection and withdrawal cycles in salt caverns: Introducing the GeoH$_2$ salt storage and cycling app, International Journal of Hydrogen Energy, https://doi.org/10.1016/j.ijhydene.2023.03.293

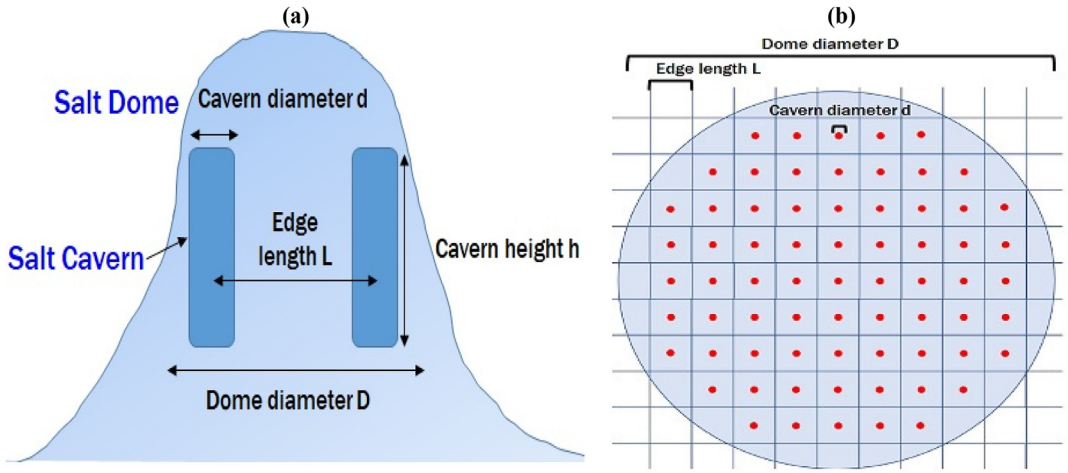


**Fig. 4 – Schematic illustrating salt caverns in a salt dome: (a) lateral view and (b) top view. The input parameters for the volumetric calculations are: (a) salt dome diameter *D*, (b) cavern diameter *d*, (c) cavern height h, (d) edge length *L* (distance between centers of adjacent caverns).**

*Geometric volume of caverns*

This work assumes that cavern geometries are either cylindrical or spherical in shape. Equation (9) computes the geometric volume of the cavern, given the cavern diameter $d$ and the cavern height $h$. If the input value for the cavern height is either empty or zero, the module performs the calculations for a spherical cavern.

$$V_{cavern} = \begin{cases} \pi\left(\frac{d}{2}\right)^2 h, h \neq 0 \\ \frac{4}{3}\pi\left(\frac{d}{2}\right)^3, h = 0 \end{cases}. \quad (9)$$

*Total geometric volume of caverns*

The total geometric volume of caverns is the multiplication of the geometric volume of a cavern $V_{cavern}$ by the effective number of caverns $n_{eff}$. The total geometric volume is the multiplication of the geometric volume of a cavern by the effective number of caverns.

$$V_{total} = n_{eff}\ V_{cavern}. \quad (10)$$

*Working gas volume per cavern*

The working gas volume of a cavern is the gas volume at standard conditions that can be withdrawn or injected (total gas volume minus cushion gas volume).

$$V_{gas\ cavern} = \left[\frac{\rho\left(T, f_{safety}\ P_{overburden}\right)}{\rho(T_{std}, P_{std})}\right](1 - f_{cushion})\ V_{cavern}. \quad (11)$$

*Total working gas volume*

The total working gas volume is the multiplication of the working gas volume of a cavern $V_{gas\ cavern}$ by the effective number of caverns $n_{eff}$. The total working volume is the summation of the working gas volume over the effective number of caverns that can be built inside a salt dome.

$$V_{gas\ total} = n_{eff}\ V_{gas\ cavern}. \quad (12)$$

*Energy per cavern*

The energy per cavern is the combustion energy of the working gas volume based on the lower heating value *LHV* per unit volume of $H_2$ (290 Btu/scf). Reference conditions for the evaluation of the *LHV* are 77 °F and 14.69 psi(a).

$$E_{cavern} = V_{gas\ cavern}\ LHV\left[\frac{\rho(77°F, P_{std})}{\rho(T_{std}, P_{std})}\right]. \quad (13)$$

*Total energy*

The total energy is the multiplication of the energy per cavern $V_{gas\ cavern}$ by the effective number of caverns $n_{eff}$.

$$E_{total} = n_{eff}\ E_{cavern}. \quad (14)$$

*Mass per cavern*

The mass per cavern is the mass of the working gas volume, which is the multiplication of the standard density $\rho_{std}$ by the working gas volume.

$$M_{cavern} = \rho(T_{std}, P_{std})\ V_{gas\ cavern}. \quad (15)$$

*Total mass*

The total mass is the multiplication of the mass per cavern $M_{cavern}$ by the effective number of caverns $n_{eff}$.

$$M_{total} = n_{eff}\ M_{cavern}. \quad (16)$$

***Production (withdrawal) calculations***

This section describes the calculations performed by the production (withdrawal) module. The module solves the unsteady-state macroscopic mass and total energy balances along with the equation of state to determine: (a) flow rate, (b)

Please cite this article as: Ruiz Maraggi LM, Moscardelli LG, Modeling hydrogen storage capacities, injection and withdrawal cycles in salt caverns: Introducing the GeoH$_2$ salt storage and cycling app, International Journal of Hydrogen Energy, https://doi.org/10.1016/j.ijhydene.2023.03.293

pressure, (c) temperature, and (d) remaining working gas at a given time. The module performs the calculations in seconds and then converts them into hours.

*Mass flow rate*

When a fluid flows through a restriction such as a pipe, the upstream (salt cavern) and downstream (pipe) conditions define the velocity. If the cavern pressure is high enough relative to the pipe pressure, the velocity will reach the speed of sound ($Ma = 1$) and the flow will be the critical flow rate. Equation (17) defines the critical pressure in terms of the upstream pressure (salt cavern pressure) and the gas isentropic exponent.

$$P_c = P\left(\frac{2}{\gamma+1}\right)^{\frac{\gamma}{\gamma-1}}, \tag{17}$$

where:

- $P_c$ is the critical pressure ($Ma = 1$).
- $P_{wf}$ is the downstream, bottomhole flowing pressure.
- $P$ is the upstream (salt cavern pressure).
- $\gamma$ is the isentropic coefficient, approximated by the heat capacity ratio $c_p/c_v$.

Equation (18) gives the mass flow rate $\dot{m}$ through an orifice for choked and non-choked conditions [23,24].

$$\dot{m} = \begin{cases} C_d\, A \sqrt{\left(\frac{2\gamma}{\gamma+1}\right) P\, \rho \left(\frac{P_c}{P}\right)^{\frac{2}{\gamma}} \left[1 - \left(\frac{P_c}{P}\right)^{\frac{\gamma-1}{\gamma}}\right]}, P_{wf} \le P_c \\ C_d\, A \sqrt{\left(\frac{2\gamma}{\gamma+1}\right) P\, \rho \left(\frac{P_{wf}}{P}\right)^{\frac{2}{\gamma}} \left[1 - \left(\frac{P_{wf}}{P}\right)^{\frac{\gamma-1}{\gamma}}\right]}, P_{wf} > P_c \end{cases}, \tag{18}$$

where:

- $\rho$ is the density of the gas at the upstream (salt cavern) conditions.
- $C_d$ is the discharge coefficient of the pipe, reference value: 0.60.
- $A$ is the cross-sectional area of the pipe.

*Unsteady-state mass balance*

Equation (19) is the macroscopic mass balance equation [14].

$$\frac{d}{dt}\int_{V_{cavern}} \rho dV_{cavern} = -\int_{A} \rho(\vec{v}\cdot\check{n})dA, \tag{19}$$

where:

- $V_{cavern}$ is the cavern volume.
- $A$ is the cross-sectional area for flow.
- $\vec{v}$ is the gas velocity in the pipe.
- $\check{n}$ is unit normal vector of the surface of the control volume.
- $t$ is the time.

Assuming uniform properties in the salt cavern we can write Eq. (19) as follows:

$$\frac{d\rho}{dt} = -\frac{\dot{m}}{V_{cavern}}. \tag{20}$$

Equation (20) gives the variation of the gas density in the cavern with time.

*Unsteady-state total energy balance*

Equation (21) is the macroscopic total energy balance equation [14].

$$\frac{d}{dt}\int_{V_{cavern}} \rho\left(\hat{u} + \frac{v^2}{2} + gz\right) dV_{cavern} = -\int_{A} \rho\left(\hat{h} + \frac{v^2}{2} + gz\right) \times (\vec{v}\bullet\check{n})dA + \dot{Q} + \dot{W}. \tag{21}$$

where:

- $\hat{u}$ is the internal energy per unit mass.
- $\frac{v^2}{2}$ is the kinetic energy per unit mass.
- $gz$ is the potential energy per unit mass.
- $\hat{h}$ is the enthalpy per unit mass.
- $\dot{Q}$ is the heat flow.
- $\dot{W}$ is the work power.

Assuming: (a) no changes in the kinetic and potential energy of the fluid, (b) no work power, and (c) uniform properties in the salt cavern, then we can write Eq. (21) as follows:

$$\frac{d(\rho\hat{u})}{dt} = -\frac{\dot{m}\hat{h}}{V_{cavern}} + \frac{\dot{Q}}{V_{cavern}}. \tag{22}$$

Using the product rule on the left side of Eq. (22):

$$\hat{u}\frac{d\rho}{dt} + \rho\frac{d\hat{u}}{dt} = -\frac{\dot{m}\hat{h}}{V_{cavern}} + \frac{\dot{Q}}{V_{cavern}}. \tag{23}$$

Inserting Eq. (20) into Eq. (23), after re-arrangement yields:

$$\frac{d\hat{u}}{dt} = \left(\frac{\dot{m}}{\rho V_{cavern}}\right)[\hat{u} - \hat{h}] + \frac{\dot{Q}}{\rho V_{cavern}}. \tag{24}$$

Recalling the definitions of the internal energy, the enthalpy, and the isentropic exponent:

$$\hat{u} = c_v T. \tag{25}$$

$$\hat{h} = c_p T. \tag{26}$$

$$\gamma = \frac{c_p}{c_v}. \tag{27}$$

Replacing Eqs. (25)–(27) into Eq. (24), after re-arrangement, produces:

$$\frac{dT}{dt} = \left(\frac{\dot{m}}{\rho V_{cavern}}\right) T[1-\gamma] + \frac{\dot{Q}}{c_v \rho V_{cavern}}. \tag{28}$$

Equation (28) gives the variation of the gas temperature $T$ in the cavern with time.

*Overall heat transfer coefficient U*

The heat flow equation is the following:

Please cite this article as: Ruiz Maraggi LM, Moscardelli LG, Modeling hydrogen storage capacities, injection and withdrawal cycles in salt caverns: Introducing the GeoH$_2$ salt storage and cycling app, International Journal of Hydrogen Energy, https://doi.org/10.1016/j.ijhydene.2023.03.293

$$\dot{Q} = U\, A_{heat}(T_i - T), \tag{29}$$

where:

- $U$ is the overall heat transfer coefficient.
- $A_{heat}$ is the area for the heat transfer.
- $T_i$ is the salt rock temperature (equal to initial cavern temperature).
- $T$ is the gas temperature in salt cavern.

Equation (30) gives the heat transfer area for cylindrical and spherical caverns, respectively:

$$A_{heat} = \begin{cases} \pi d h & h \neq 0 \\ \pi d^2 & h = 0 \end{cases}. \tag{30}$$

This work considers both the natural convection heat transfer coefficient of the gas in the cavern $h_{con}$ and the heat conduction in the salt rock surrounding the salt cavern $k_{salt}$. Equation (31) gives the overall heat transfer coefficient (referred to the cavern internal diameter $d$) for cylindrical and spherical caverns, respectively:

$$U = \begin{cases} \dfrac{1}{\dfrac{1}{h_{con}} + \dfrac{d}{2k_{salt}} ln\left(\dfrac{d_0}{d}\right)} & h \neq 0 \\ \dfrac{1}{\dfrac{1}{h_{con}} + \dfrac{d^2}{2k_{salt}}\left[\dfrac{1}{d} - \dfrac{1}{d_0}\right]} & h = 0 \end{cases}, \tag{31}$$

where $d_0$ is the external diameter at which the rock salt temperature remains constant. This study assumes $d_0 = 3.28\, ft + d$.

*$H_2$ convective heat transfer coefficient h*

The heat transfer coefficient for systems subject to depressurization is modeled using natural convection. This section presents the correlations to estimate the natural convection heat transfer coefficient of the gas in the cavern $h_{con}$. The natural heat convection coefficient depends on the geometry of the salt cavern. Therefore, this section presents the heat transfer coefficient for both cylindrical and spherical caverns.

- **Cylindrical Systems**

For cylindrical systems, [25] presents an empirical correlation for calculating the natural convection heat transfer coefficient of hydrogen:

$$Nu = 0.104\, Ra^{0.352}, \tag{32}$$

where:

- $Nu$ is the Nusselt dimensionless number.
- $Ra$ is the Rayleigh dimensionless number.

- **Spherical Systems**

For spherical systems, [26] presents an empirical correlation for calculating the natural convection heat transfer coefficient:

$$Nu = 2 + \frac{0.589 Ra^{0.25}}{\left[1 + \left(\frac{0.469}{Pr}\right)^{9/16}\right]^{4/9}}, \tag{33}$$

where $Pr$ is the Prandtl dimensionless number.

For both cylindrical and spherical systems, the fluid properties should be evaluated at the film temperature $T_{film}$.

$$T_{film} = \frac{T_i + T}{2}. \tag{34}$$

*Injection calculations*

Given the cavern geometry, initial cavern conditions (pressure and temperature), maximum working pressure, and a constant injection rate and injection temperature, this module estimates:

1. Cavern pressure with time.
2. Cavern temperature with time.
3. Working gas (total gas volume minus cushion gas volume) in cavern with time.

The module performs the calculations until the pressure in the cavern equals the maximum allowable working pressure.

The module can perform the calculations for cylindrical and spherical salt caverns.

*Unsteady-state mass balance*

The macroscopic mass balance is:

$$\frac{d\rho}{dt} = \frac{\dot{m}}{V_{cavern}}. \tag{35}$$

*Unsteady-state total energy balance*

Using the same assumptions as in the production module, the macroscopic total energy balance is:

$$\frac{d\hat{u}}{dt} = \left(\frac{\dot{m}}{\rho V_{cavern}}\right)[\hat{h} - \hat{u}] + \frac{\dot{Q}}{\rho V_{cavern}}. \tag{36}$$

Replacing Eqs. (25)–(27) into Eq. (36), after re-arrangement, produces:

$$\frac{dT}{dt} = \left(\frac{\dot{m}}{\rho V_{cavern}}\right)[\gamma T_{inj} - T] + \frac{\dot{Q}}{c_v \rho V_{cavern}}. \tag{37}$$

Equation (37) gives the variation of the gas temperature $T$ in the cavern with time.

*$H_2$ convective heat transfer coefficient h*

The heat transfer coefficient for systems subject to filling is modeled by combined natural and forced convection (mixed

Please cite this article as: Ruiz Maraggi LM, Moscardelli LG, Modeling hydrogen storage capacities, injection and withdrawal cycles in salt caverns: Introducing the GeoH$_2$ salt storage and cycling app, International Journal of Hydrogen Energy, https://doi.org/10.1016/j.ijhydene.2023.03.293

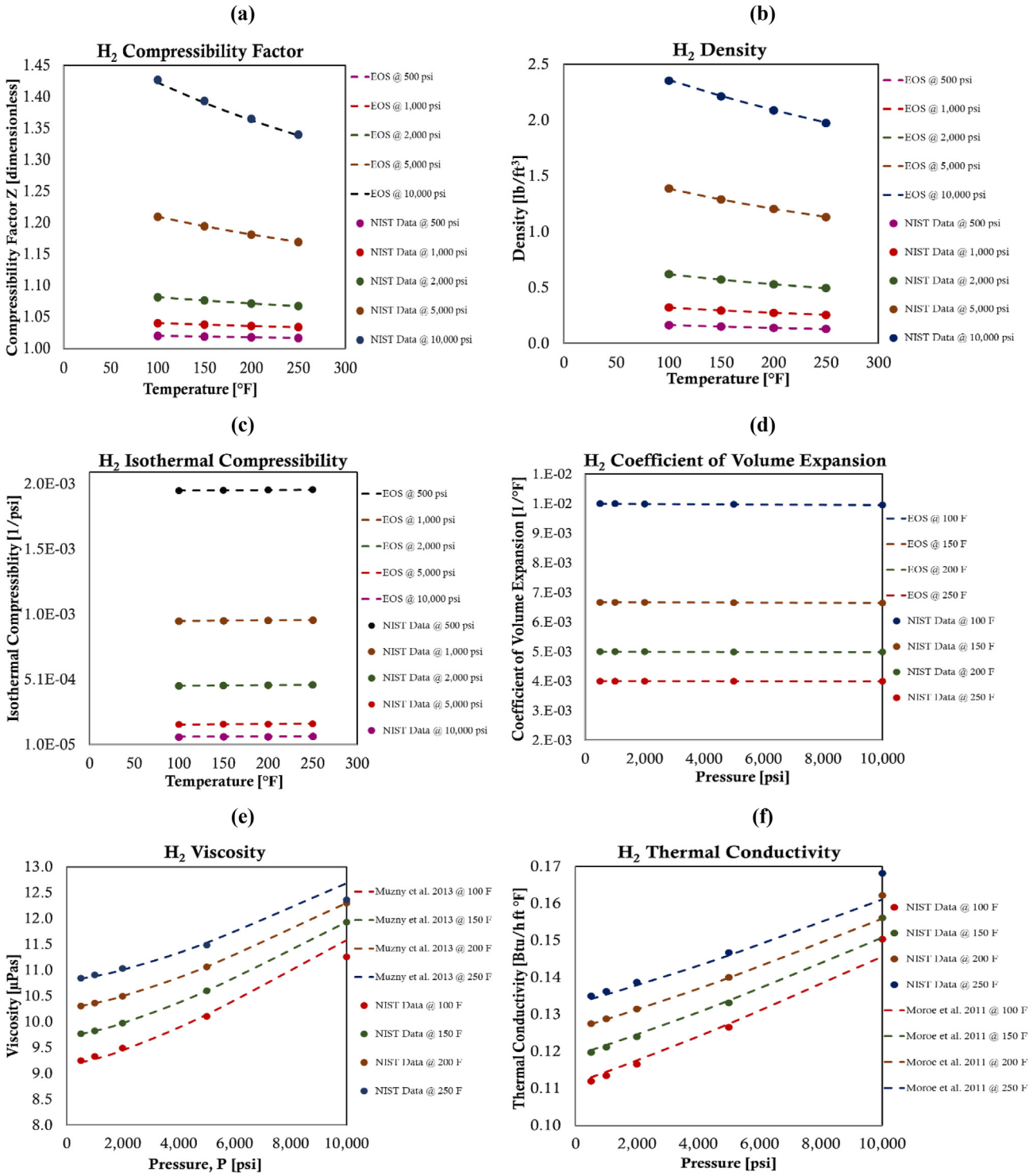


**Fig. 5 – Validation of the correlations used in this work (dashed curves) against $H_2$ data (solid dots) from the National Institute of Standards and Technology: (a) compressibility factor, (b) density, (c) isothermal compressibility, (d) coefficient of volume expansion, (e) viscosity, and (f) thermal conductivity.**

convection). This section presents the correlations that estimate the mixed convection heat transfer coefficient of the gas in the cavern $h_{mix\ con}$. The mixed heat convection coefficient depends on the geometry of the salt cavern. Therefore, this section presents the heat transfer coefficient for both cylindrical and spherical caverns.

- **Cylindrical Systems**

Please cite this article as: Ruiz Maraggi LM, Moscardelli LG, Modeling hydrogen storage capacities, injection and withdrawal cycles in salt caverns: Introducing the GeoH$_2$ salt storage and cycling app, International Journal of Hydrogen Energy, https://doi.org/10.1016/j.ijhydene.2023.03.293

**Table 1 – Hydrogen storage data in salt caverns [22].**

| Parameter/Salt Name | Simone | Clemens | Moss Bluff | Spindeltop | Teeside |
|---|---|---|---|---|---|
| Cavern geometry | cylindrical | cylindrical | cylindrical | cylindrical | spherical |
| Edge length [ft] | 600 | N/A | N/A | N/A | N/A |
| Salt Dome diameter [ft] | 6262 | N/A | N/A | N/A | N/A |
| Maximum working pressure [psi] | 1400 | 1110 | 1755 | 2553 | 641 |
| Geometric volume [MMft$^3$] | 15.70 | 20.48 | 19.99 | 32.00 | 2.47 |
| Number of caverns | N/A | 1 | 1 | 1 | 3 |
| Fraction of caverns being built | 0.50 | N/A | N/A | N/A | N/A |
| Fraction of cushion gas | 0.30 | N/A | N/A | N/A | N/A |

**Table 2 – Comparison of the volumetric module calculations and the data reported by Ref. [22]. The actual data and the calculated values are in good agreement, showing less than 10% relative error. These small differences relate to missing input data such as fraction of cushion gas volume, cavern temperature, and maximum allowable working pressure.**

| Salt Name/Example | Parameter | Data | Volumetric Calculation | Relative Error [%] |
|---|---|---|---|---|
| Simone et al., 2021 | Total number of caverns | 63.00 | 63.00 | 0.00% |
| | Effective number of caverns | 31.00 | 31.00 | 0.00% |
| | Geometric volume cavern [MMft$^3$] | 15.70 | 15.71 | 0.06% |
| | Working gas cavern [BSft$^3$] | 1.05 | 0.938 | −10.67% |
| | Hydrogen mass cavern [Ton] | 2482.00 | 2258.00 | −9.02% |
| | Total hydrogen mass [Ton] | 76,950.00 | 69,986.00 | −9.05% |
| Clemens | Geometric volume cavern [MMft$^3$] | 20.48 | 20.48 | 0.00% |
| | Working gas cavern [BSft$^3$] | 0.96 | 0.96 | 0.00% |
| | Energy per cavern [GWh] | 81.00 | 77.28 | −4.59% |
| | Hydrogen mass cavern [Ton] | 2400.00 | 2319.13 | −3.37% |
| Moss Bluff | Geometric volume cavern [MMft$^3$] | 19.99 | 19.99 | 0.00% |
| | Working gas cavern [BSft$^3$] | 1.47 | 1.45 | −1.36% |
| | Energy per cavern [GWh] | 120.00 | 116.33 | −3.06% |
| | Hydrogen mass cavern [Ton] | 3690.00 | 3490.93 | −5.39% |
| SpindelTop | Geometric volume cavern [MMft$^3$] | 32.00 | 32.00 | 0.00% |
| | Working gas cavern [BSft$^3$] | 3.27 | 3.27 | 0.00% |
| | Energy per cavern [GWh] | 262.84 | 274 | 4.25% |
| | Hydrogen mass cavern [Ton] | 8230.00 | 7866.00 | −4.42% |
| Teeside | Geometric volume cavern [MMft$^3$] | 2.47 | 2.47 | 0.00% |
| | Total geometric volume [BSft$^3$] | 7.42 | 7.42 | 0.00% |
| | Total Energy [GWh] | 27.00 | 25.00 | −7.41% |
| | Total Hydrogen mass [Ton] | 810.00 | 759.28 | −6.26% |

For cylindrical systems, [27] presents an empirical correlation for calculating the mixed convection heat transfer coefficient of hydrogen:

$$Nu_{mix\ conv} = 0.56Re^{0.67} + 0.104\,Ra^{0.352}, \quad (38)$$

where:

- $Nu_{mix\ conv}$ is the mixed convection Nusselt dimensionless number.
- $Ra$ is the Rayleigh dimensionless number.
- $Re$ is the Reynolds dimensionless number.

- **Spherical Systems**

**Table 3 – Inputs for the validation of the GeoH$_2$ production module validation using HyDown thermodynamic simulator [29].**

| Input/Example | Case 1 | Case 2 | Case 3 |
|---|---|---|---|
| Initial pressure $P_i$ [psi] | 2466 | 2973 | 2176 |
| Initial temperature $T_i$ [°F] | 140 | 122 | 122 |
| Final operating pressure $P_{final}$ [psi] | 723 | 1208 | 458 |
| Bottomhole flowing pressure $P_{wf}$ [psi] | 145 | 435 | 145 |
| Height, h [ft] | 804 | 574 | 918 |
| Diameter, d [ft] | 230 | 164 | 115 |
| Fraction of cushion gas $f_{cushion}$ | 0 | 0 | 0 |
| Tubing internal diameter, $d_{tubing}$ [in] | 3.46 | 3.46 | 3.46 |
| Discharge coefficient, $Cd$ | 1 | 1 | 1 |

Please cite this article as: Ruiz Maraggi LM, Moscardelli LG, Modeling hydrogen storage capacities, injection and withdrawal cycles in salt caverns: Introducing the GeoH$_2$ salt storage and cycling app, International Journal of Hydrogen Energy, https://doi.org/10.1016/j.ijhydene.2023.03.293

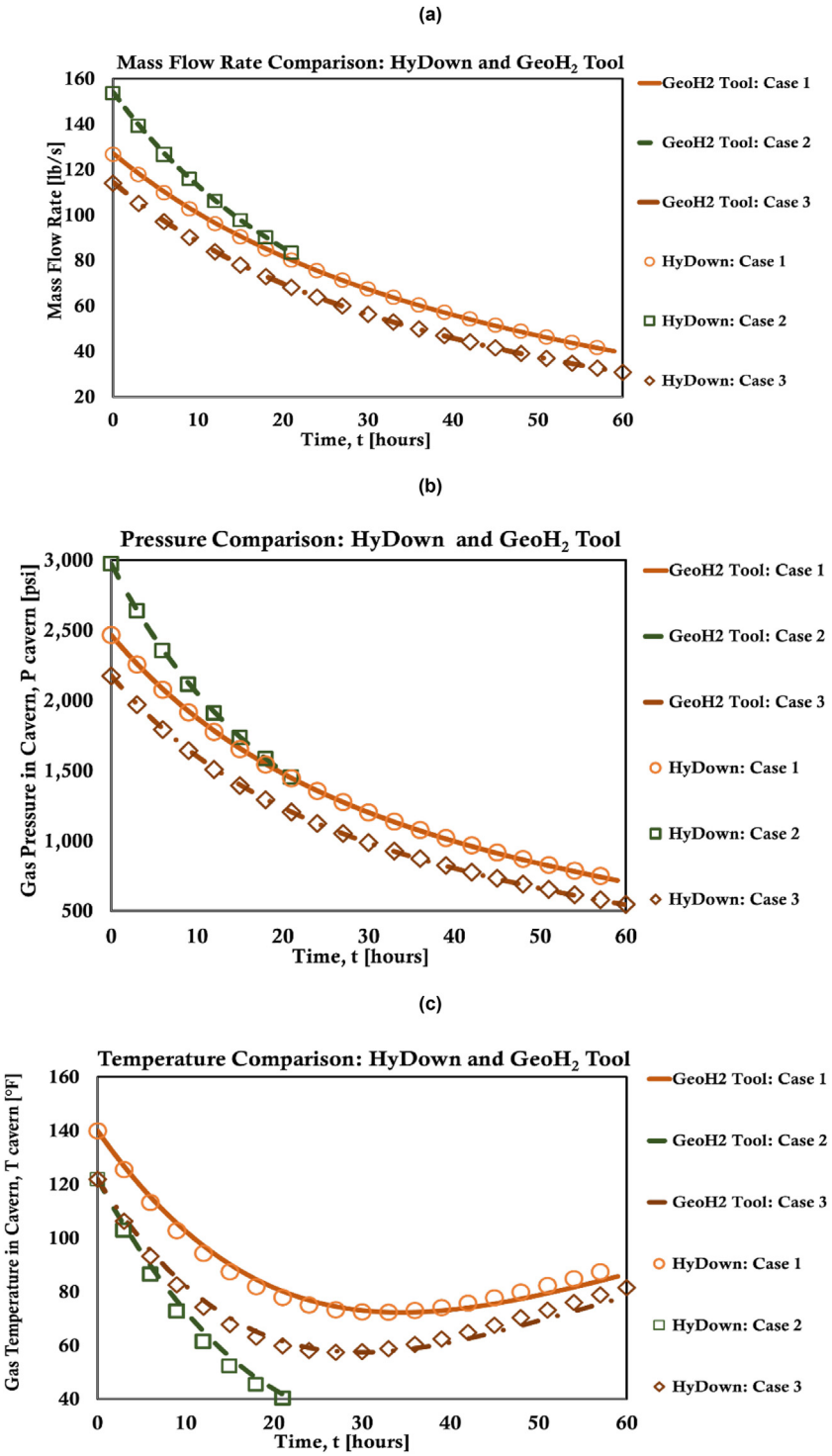


**Fig. 6 – Comparison of GeoH2 and HyDown results in terms of: (a) mass flow rate, (b) pressure, and (c) temperature for the four simulation cases presented in Table 3. There is an excellent agreement between the results of both simulators.**

For spherical systems, [26] presents an empirical correlation for calculating the mixed convection heat transfer coefficient using natural and forced convection correlations:

$$Nu_{mix\ conv}{}^3 = Nu_{conv}{}^3 + Nu_{forced}{}^3, \quad (39)$$

where:

- $Nu_{mix\ conv}$ is Nusselt dimensionless number for mixed convection.
- $Nu_{conv}$ is Nusselt dimensionless number for natural convection.
- $Nu_{forced}$ is Nusselt dimensionless number for forced convection.

Please cite this article as: Ruiz Maraggi LM, Moscardelli LG, Modeling hydrogen storage capacities, injection and withdrawal cycles in salt caverns: Introducing the GeoH$_2$ salt storage and cycling app, International Journal of Hydrogen Energy, https://doi.org/10.1016/j.ijhydene.2023.03.293

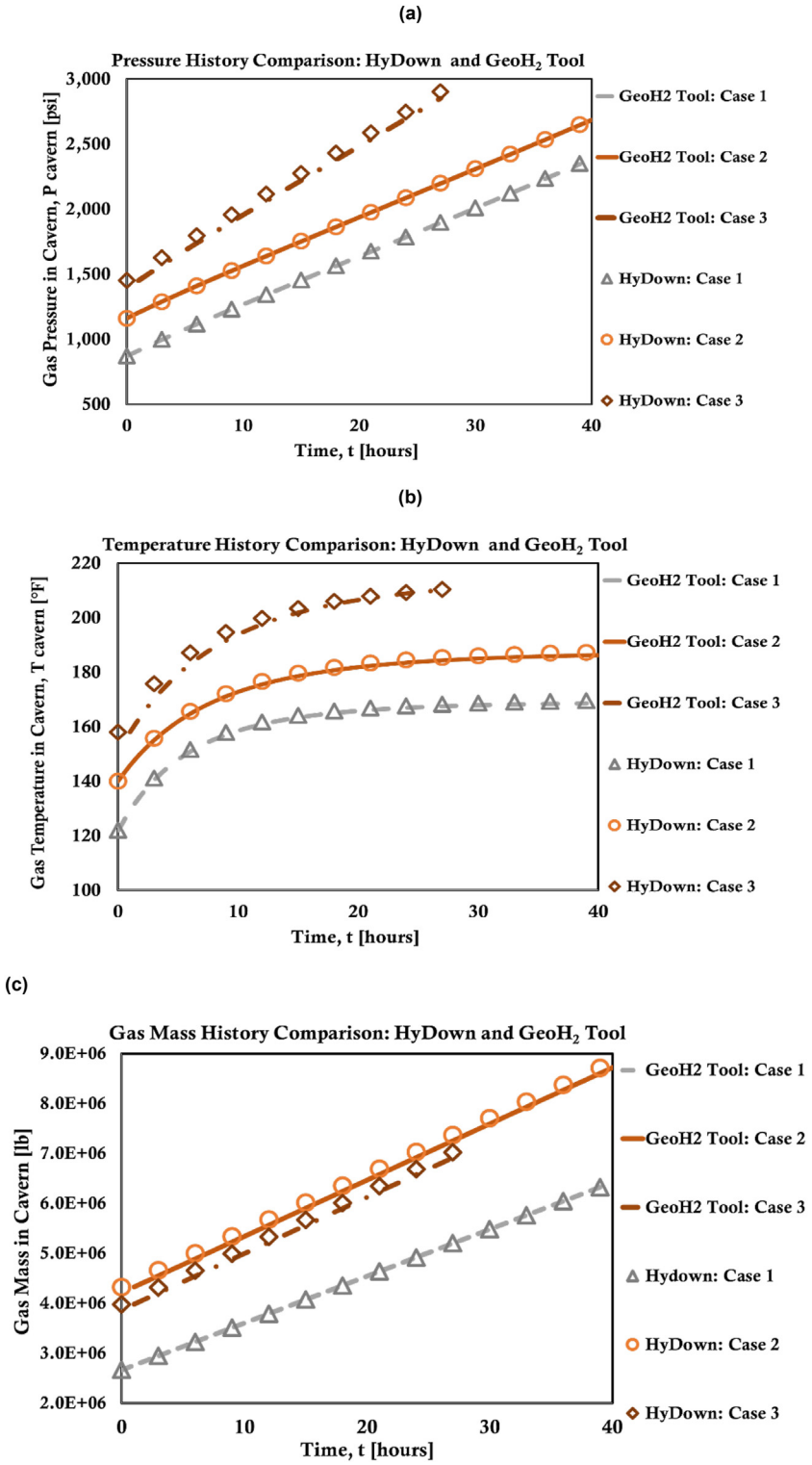


**Fig. 7 – Comparison of $GeoH_2$ and HyDown results in terms of: (a) pressure, (b) temperature, and (c) gas in cavern for the four simulation cases presented in Table 4. There is an excellent agreement between the results of both simulators.**

Please cite this article as: Ruiz Maraggi LM, Moscardelli LG, Modeling hydrogen storage capacities, injection and withdrawal cycles in salt caverns: Introducing the $GeoH_2$ salt storage and cycling app, International Journal of Hydrogen Energy, https://doi.org/10.1016/j.ijhydene.2023.03.293

**Table 4 – Inputs for the validation of the GeoH$_2$ injection module validation using HyDown thermodynamic simulator.**

| Input/Example | Case 1 | Case 2 | Case 3 |
|---|---|---|---|
| Initial pressure $P_i$ [psi] | 870 | 1160 | 1450 |
| Initial temperature $T_i$ [°F] | 122 | 140 | 158 |
| Maximum operating pressure $P_{final}$ [psi] | 2350 | 2878 | 2850 |
| Injection rate, $q_{inj}$ [MMScf/h] | 17.66 | 21.19 | 21.19 |
| Height, h [ft] | 725 | 919 | 919 |
| Diameter, d [ft] | 131 | 131 | 115 |
| Fraction of cushion gas $f_{cushion}$ | 0 | 0 | 0 |
| Tubing internal diameter, $d_{tubing}$ [in] | 3.46 | 3.46 | 3.46 |

Equations (40) and (41) give the natural and forced convection correlations, respectively.

$$Nu_{conv} = 2 + \frac{0.589Ra^{0.25}}{\left[1+\left(\frac{0.469}{Pr}\right)^{9/16}\right]^{4/9}}. \quad (40)$$

$$Nu_{forced} = 2 + 0.60Re^{1/2}\,Pr^{1/3}, \quad (41)$$

where:

- $Pr$ is the Prandtl dimensionless number.
- $Re$ is the Reynolds dimensionless number.

For both cylindrical and spherical systems, the fluid properties should be evaluated at the film temperature $T_{film}$.

### *Cycling calculations*

This cycling module that simulates the sequential withdrawal and injection processes of $H_2$ in salt caverns. The module uses the equations of the production and injection modules, respectively.

## Results and discussion

This section presents the validation of the different modules.

### *Fluid properties module*

This study validates the results of the correlations used in the fluid properties and subsequent modules against $H_2$ data from the from the National Institute of Standards and Technology (NIST) [28].

Fig. 5 illustrates the validation of the correlations used in this work against $H_2$ data from NIST [28] for different pressures and temperatures for the following $H_2$ physical properties: **(a)** compressibility factor, **(b)** density, **(c)** isothermal compressibility, **(d)** coefficient of volume expansion, **(e)** viscosity, and **(f)** thermal conductivity. There is an excellent agreement between the empirical data and the correlations used in this work.

### *Volumetric module*

This section validates the calculations of the volumetric module against real $H_2$ storage data in salt caverns. Table 1 presents the data for salt caverns that store $H_2$ [22].

Table 2 compares the results of the volumetric module calculations and the data reported by Ref. [22] for these salt caverns. The actual data and the calculated values are in good agreement, showing less than 10% relative error. These small differences relate to missing input data such as fraction of cushion gas volume, cavern temperature, and maximum allowable working pressure.

### *Production module*

This section shows the validation of the production calculations using an open-source real gas thermodynamic simulator (HyDown) built for $H_2$ injection and withdrawal in pressurized cylindrical vessels [29]. The main differences between the HyDown software and the GeoH$_2$ are the following. First, our software is specifically designed to model heat-transfer between hydrogen in the cavern and the salt rock mass for both cylindrical and spherical caverns. In contrast, HyDown software models heat transfer between hydrogen and the air surrounding the pressurized vessel. Second, HyDown software does not account for cushion gas

**Table 5 – Initial conditions and three production and withdrawal processes for the cycling simulation results shown in Fig. 8.**

| Input/Example | | | | | | | Case 1 |
|---|---|---|---|---|---|---|---|
| Initial pressure $P_i$ [psi] | | | | | | | 4000 |
| Initial temperature $T_i$ [°F] | | | | | | | 100 |
| Maximum operating $P_{final}$ [psi] | | | | | | | 4000 |
| Height, h [ft] | | | | | | | 1000 |
| Diameter, d [ft] | | | | | | | 100 |
| Fraction of cushion gas $f_{cushion}$ | | | | | | | 0.30 |
| Tubing internal diameter, $d_{tubing}$ [in] | | | | | | | 3.46 |
| Discharge coefficient, $Cd$ | | | | | | | 0.60 |
| Variable/Process | **Production** | **Injection** | **Production** | **Injection** | **Production** | **Injection** | **Production** |
| Final pressure [psi] | | 4000 | | 4000 | | 4000 | |
| Injection rate [MMScf/h] | | 10 | | 10 | | 10 | |
| Final pressure [psi] | 2000 | | 2000 | | 2000 | | 2000 |
| Bottomhole pressure [psi] | 1500 | | 1500 | | 1500 | | 1500 |

Please cite this article as: Ruiz Maraggi LM, Moscardelli LG, Modeling hydrogen storage capacities, injection and withdrawal cycles in salt caverns: Introducing the GeoH$_2$ salt storage and cycling app, International Journal of Hydrogen Energy, https://doi.org/10.1016/j.ijhydene.2023.03.293

volume fraction. Third, the $GeoH_2$ app is a modular application specifically designed to model storage, withdrawal, injection, and sequential cycling of $H_2$ in salt caverns allowing the user to estimate storage capacities in salt domes and to simulate sequential injection and withdrawal processes in salt caverns. HyDown lacks these features.

Here we compare the results for 3 different cases based on a constant overall heat transfer coefficient using the $GeoH_2$ Storage and Cycling App and the HyDown open software in terms of the mass flow rate, pressure, and temperature.

Table 3 shows the inputs for the simulations using the $GeoH_2$ and HyDown software.

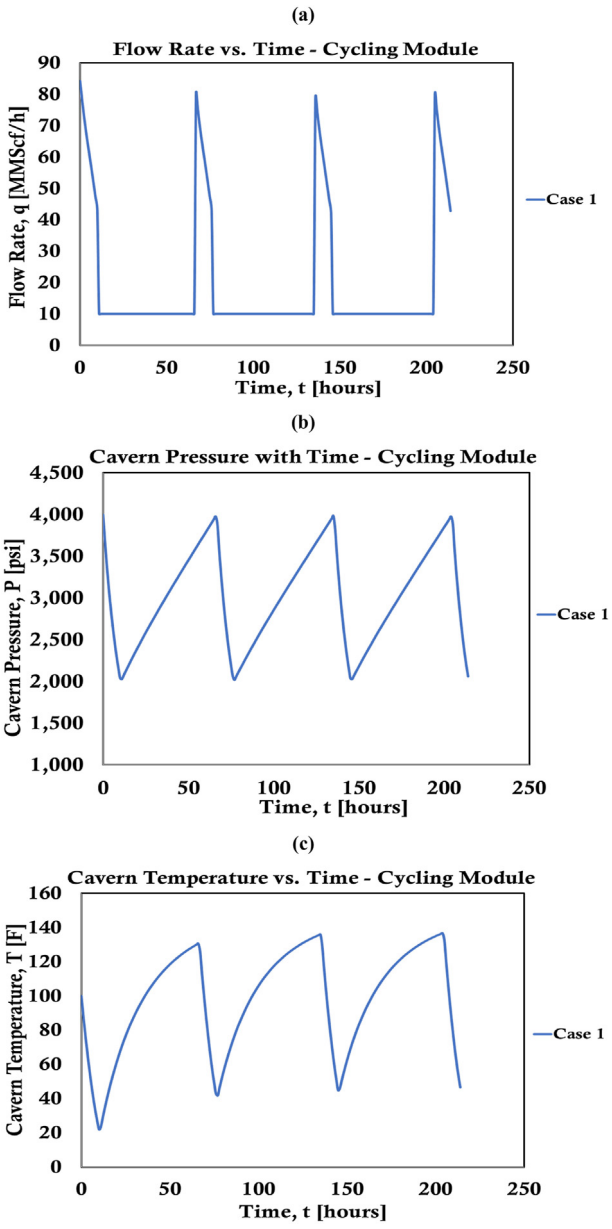


**Fig. 8 – Results of the cycling module simulation in terms of: (a) flow rate, (b) cavern pressure, and (c) cavern temperature histories for input parameters presented in Table 5.**

Fig. 6 illustrates the comparison of $GeoH_2$ and HyDown [29] results in terms of: **(a)** pressure, **(b)** temperature, and **(c)** gas in cavern with time. There is an excellent agreement between the simulations performed by the $GeoH_2$ app and the HyDown software.

### *Injection module*

This section presents the validation of the injection calculations using an open-source real gas hydrogen thermodynamic simulator: HyDown [29]. Here, we compare the results for 3 different cases based on a constant overall heat transfer coefficient using the $GeoH_2$ Storage and Cycling App and the HyDown open software in terms of the pressure, the temperature, and the gas in cavern.

Table 4 shows the inputs for the simulations using the $GeoH_2$ and HyDown software.

Fig. 7 illustrates the comparison of $GeoH_2$ and HyDown [29] results in terms of: **(a)** mass flow rate, **(b)** pressure, and **(c)** temperature. There is an excellent agreement between the simulations performed by the $GeoH_2$ app and the HyDown software.

### *Cycling module*

This section illustrates the cycling module capabilities. This module allows the user to simulate sequential injection and withdrawal cycles in salt cavern. Table 5 illustrate the initial cavern conditions and three production and withdrawal cycles for the cycling simulation.

Fig. 8 illustrates the results of the simulation in terms of the: (a) flow rate, (b) cavern pressure, and (c) cavern temperature.

## Conclusions

This work presented the development, the validation, and the application of a novel software tool suitable to assess the technical potential of $H_2$ for storage, injection, withdrawal, and cycling operations in salt caverns. Future work plans to incorporate geomechanical effects to assess salt cavern stability during withdrawal and injection operations and economic analysis to evaluate capital and operating expenditures during the construction and operation of salt caverns.

The pressing urgency to accelerate the development of a viable $H_2$ economy to mitigate the adverse effects of climate change will require a better understanding of our real capacity to store hydrogen in the subsurface and the effects of rapid $H_2$ injection/withdrawal cycles. Rapid changes in flow rates, cavern pressures and temperatures will pose engineering challenges that need to be carefully assessed so that product loss and contamination can be avoided and for safety considerations. Hydrogen storage in salt caverns has been categorized as a proven technology; however, the use of $H_2$ as an energy carrier broadens the scope of use beyond refinery processes and the manufacture of fertilizers. There are many above and below technical challenges that still need to be tackle using both engineering and geoscience approaches.

Please cite this article as: Ruiz Maraggi LM, Moscardelli LG, Modeling hydrogen storage capacities, injection and withdrawal cycles in salt caverns: Introducing the $GeoH_2$ salt storage and cycling app, International Journal of Hydrogen Energy, https://doi.org/10.1016/j.ijhydene.2023.03.293

## Declaration of competing interest

The authors declare that they have no known competing financial interests or personal relationships that could have appeared to influence the work reported in this paper.

## Acknowledgements

This work has been funded by the State of Texas Advanced Resource Recovery (STARR) program. The authors want to thank Mark Shuster and members of the $GeoH_2$ consortium at the Bureau of Economic Geology for supporting this work and for insightful discussions. Publication authorized by the director, Bureau of Economic Geology, The University of Texas at Austin.

## Nomenclature and Units

| | |
|---|---|
| $A$ | cross-sectional area for fluid flow, $L^2$, $ft^2$ |
| $A_{heat}$ | heat transfer area $L^2$, $ft^2$ |
| $c_g$ | isothermal compressibility, $Lt^2/m$, $psi^{-1}$ |
| $c_p$ | heat capacity per unit mass at constant pressure, $L^2/(T\ t^2)$, Btu/(lb °F) |
| $c_v$ | heat capacity per unit mass at constant volume, $L^2/(T\ t^2)$, Btu/(lb °F) |
| $C_d$ | discharge coefficient, dimensionless |
| $d$ | cavern diameter, L, ft |
| $d_0$ | cavern outer diameter at which the temperature is the salt rock temperature, L, ft |
| $d_{tubing}$ | tubing internal diameter, L, ft |
| $D$ | salt dome edge length, L, ft |
| $E_{cavern}$ | combustion energy per cavern, $mL^2/t^2$, GWh |
| $E_{total}$ | total combustion energy, $mL^2/t^2$, GWh |
| $f_{built}$ | fraction of caverns built, fraction |
| $f_{cushion}$ | fraction of cushion gas, fraction |
| $f_{safety}$ | safety factor for calculatingthe maximum allowable working pressure, fraction |
| $h$ | cavern height, L, ft |
| $h_{con}$ | natural convection heat transfer coefficient, $m/(Tt^3)$, $BTU/(h\ ft^{2\circ})$ |
| $h_{mix\ con}$ | nixed convection heat transfer coefficient, $m/(Tt^3)$, $BTU/(h\ ft^{2\circ})$ |
| $k$ | gas thermal conductivity, $mL/(Tt^3)$, BTU/(h ft °F) |
| $k_{salt}$ | Salt rock thermal conductivity thermal conductivity, $mL/(Tt^3)$, BTU/(h ft °F) |
| $L$ | edge length, L, ft |
| $\dot{m}$ | mass flow rate, m/t, lb/s |
| $M_{cavern}$ | mass per cavern, m, Ton |
| $M_{total}$ | total mass, m, Ton |
| $M_r$ | hydrogen molecular weight, lb/lbmol |
| $Ma$ | Mach dimensionless number |
| $n$ | total number of caverns, number |
| $Nu$ | Nusselt number, dimensionless |
| $P$ | pressure, $m/(L\ t^2)$, psi |
| $Pr$ | Prandtl number, dimensionless |
| $R$ | ideal gas constant, $m\ L^2/(T\ t^2)$, Btu $R^{-1}$ $lbmol^{-1}$ |
| $Ra$ | Rayleigh number, dimensionless |
| $Re$ | Reynolds number, dimensionless |
| $t$ | time, t, seconds |
| $T$ | temperature, T, °F, R |
| $T_i$ | initial cavern temperature or salt rock mass temperature, T, °F, R |
| $T_{inj}$ | temperature of the injected hydrogen into the cavern, T, °F, R |
| $\upsilon$ | velocity, L/t, ft/s |
| $V$ | gas volume, $L^3$, $ft^3$ |
| $V_{cavern}$ | geometric volume of cavern, $L^3$, $ft^3$ |
| $V_{total}$ | total geometric volume, $L^3$, $ft^3$ |
| $Z$ | compressibility factor, dimensionless |
| $\beta$ | coefficient of volume expansion, $T^{-1}$, $°F^{-1}$ |
| $\gamma$ | isentropic coefficient, dimensionless |
| $\mu$ | viscosity, m/Lt, μcp |
| $\rho$ | density, $m/L^3$, $lb/ft^3$ |

## REFERENCES

[1] Shuster M, Bhattacharya S, Duncan IJ, et al. Hydrogen infrastructure expansion requires realistic framework. Oil Gas J 2021;119(5). https://www.ogj.com/pipelines-transportation/article/14202928/hydrogen-infrastructure-expansion-requires-realistic-framework.

[2] Matos CR, Carneiro JL, Silvia PP. Overview of large-scale underground energy storage technologies for integration of renewable energies and criteria for reservoir identification. J Energy Storage 2019;21:241–58. https://doi.org/10.1016/j.est.2018.11.023.

[3] Crotogino F, Schneider GS, Evans D. Renewable energy storage in geological formations. J Power Energy 2018;232(1):100–14. https://doi.org/10.1177/0957650917731181.

[4] Fundación Hidrógeno Aragón. Hyunder: assessing the potential, actors, and business models of large-scale underground hydrogen storage in Europe. http://hyunder.eu/ [Accessed 15 March 2023].

[5] Kruck O, Crotogino F. Hyunder: assessing the potential, actors, and business models of large-scale underground hydrogen storage in Europe. Benchmark of selected storage options. http://hyunder.eu/wp-content/uploads/2016/01/D3.3_Benchmarking-of-selected-storage-options.pdf[Accessed 15 March 2023].

[6] Hypster: hydrogen storage. https://hypster-project.eu/ [Accessed 15 March 2023].

[7] Wang G, Pickup G, Sorbie K, Mackay E. Numerical modelling of $H_2$ storage with cushion gas of $CO_2$ in subsurface porous media: filter effects of $CO_2$ solubility. Int J Hydrogen Energy 2022;47(67):28956–68. https://doi.org/10.1016/j.ijhydene.2022.06.201.

[8] Luboń K, Tarkowski R. Numerical simulation of hydrogen injection and withdrawal to and from a deep aquifer in NW Poland. Int J Hydrogen Energy 2020;45(3):2068–83. https://doi.org/10.1016/j.ijhydene.2019.11.055.

[9] Cai Z, Zhang K, Guo C. Development of a novel simulator for modeling underground hydrogen and gas mixture storage. Int J Hydrogen Energy 2022;47:8929–42. https://doi.org/10.1016/j.ijhydene.2021.12.224.

[10] Berest P. Heat transfer in salt caverns. Int J Rock Mech Min Sci 2019;120:82–95. https://doi.org/10.1016/j.ijrmms.2019.06.009.

[11] Berest P, Louvet F. Aspects of the thermodynamic behavior of salt caverns used for gas storage. Oil Gas Sci Technol – Rev

IFP Energies nouvelles 2020;75:57. https://doi.org/10.2516/ogst/2020040.
[12] Bérest P, Brouard B, Karimi-Jafari M, Van Sambeek L. Transient behavior of salt. Int J Rock Mech Min Sci 2007;44(5):767–86. https://doi.org/10.1016/j.ijrmms.2006.11.007.
[13] Berest P, Djakeun-Djizanne H, Brouard B, Hévin G. Rapid depresurizations: can they lead to irreversible damage?. In: SMRI Spring Conference, 23–24 april 2012, Regina, Apr 2012, Canada; 2012. p. 63–86. ⟨hal-00787107⟩.
[14] Bird RB, Stewart WE, Lightfoot EN. Transport phenomena. 2nd ed. Hoboken, New Jersey: John Wiley & Sons; 2002.
[15] Gupta RB, Basile A, Veziroğlu TN. Compendium of hydrogen energy volume 2: hydrogen storage, transportation and infrastructure. In: Woodhead Publishing Series in Energy 2016; 2016. p. 91–115. https://doi.org/10.1016/B978-1-78242-362-1.00004-3.
[16] Li J, Shi X, Yang C, et al. Mathematical model of salt cavern leaching for gas storage in high-insoluble salt formations. Sci Rep 2018;8(372):1–12. https://doi.org/10.1038/s41598-017-18546-w.
[17] Raymond J, Langevin H, Comeau FH, et al. Temperature dependence of rock salt thermal conductivity: implications for geothermal exploration. Renew Energy 2022;184:26–35. https://doi.org/10.1016/j.renene.2021.11.080.
[18] Lemmon E, Huber ML, Leachman JW. Revised standardized equation for hydrogen gas densities for fuel consumption applications. J. Res. Natl. Inst. Stand. Technol. 2008;113:341–50. https://doi.org/10.6028/jres.113.028.
[19] Smith JM, Van Ness HC, Abbott MM, Swihart MT. Introduction to chemical engineering thermodynamics. eight edition. New York, USA: Mc Graw Hill; 2018.
[20] Muzny CD, Huber ML, Kazakov AF. Correlation for the viscosity of normal hydrogen obtained from symbolic regression. J Chem Eng Data 2013;58(4):969–79. https://doi.org/10.1021/je301273j.
[21] Moroe S, Woodfield PL, Kimura K, et al. Measurements of hydrogen thermal conductivity at high pressure and high temperature. Int J Thermophys 2011;32:1887–917. https://doi.org/10.1007/s10765-011-1052-5.
[22] Simone A, Morisani-Zechmeister A, Frey F. Preparing for a hydrogen future – constraints and alternatives for hydrogen storage. Solution mining research institute fall 2021. USA: Galveston, TX; 2021. Technical Conference. 20-21 September.
[23] Sallet DW, Palmer ME. The non-steady flow of gases and vapours from pressure vessels. Proc Inst Mech Eng 1980;194(1):225–30. https://doi.org/10.1243/PIME_PROC_1980_194_027_02.
[24] Saad MA. Compressible fluid flow. 1st ed. New Jersey, USA: Prentice-Hall; 1993.
[25] Daney DE. Turbulent natural convection of liquid deuterium, hydrogen, and nitrogen within enclosed vessels. Int J Heat Mass Tran 1976;19:431–41. https://doi.org/10.1016/0017-9310(76)90099-5.
[26] Bergman T, Lavine A. Fundamentals of heat and mass transfer. 8th ed. Hoboken, New Jersey: John Wiley & Sons; 2017.
[27] Woodfield PL, Monde M, Mitsutake Y. Measurement of averaged heat transfer coefficients in high-pressure vessel during charging with hydrogen, nitrogen or argon gas. J Therm Sci Technol 2006;2(2):180–90. https://doi.org/10.1299/jtst.2.180.
[28] Lemmon EW, Bell IH, Huber ML, McLinden MO. NIST standard reference database 23: reference fluid thermodynamic and transport properties-REFPROP, Version 10.0. Gaithersburg: National Institute of Standards and Technology, Standard Reference Data Program; 2018. https://doi.org/10.18434/T4/1502528.
[29] Andreasen A. HyDown: a Python package for calculation of hydrogen (or other gas) pressure vessel filling and discharge. J Open Source Softw 2021;6(66):1–6. https://doi.org/10.21105/joss.03695.

Please cite this article as: Ruiz Maraggi LM, Moscardelli LG, Modeling hydrogen storage capacities, injection and withdrawal cycles in salt caverns: Introducing the GeoH$_2$ salt storage and cycling app, International Journal of Hydrogen Energy, https://doi.org/10.1016/j.ijhydene.2023.03.293